A higher order scheme for two-dimensional quasi-static crack growth simulations

Englund, Jonas

Published in:
Computer Methods in Applied Mechanics and Engineering

DOI:
10.1016/j.cma.2007.01.007

2007

Quasi-static crack growth simulations

J. Englund [1]

Numerical Analysis, Centre for Mathematical Sciences, Lund University,
Box 118, SE-221 00, Lund, Sweden.

Abstract

An efficient scheme for the simulation of quasi-static crack growth in two-dimensional linearly elastic isotropic specimens is presented. The crack growth is simulated in a stepwise manner where an extension to the already existing crack is added in each step. In a local coordinate system each such extension is represented as a polynomial of some, user specified, degree, n. Denote an extension by Γ^{ext}, where $\Gamma^{\text{exp}} = \{(x, y(x)) : 0 \leq x \leq h\}$, where x and y are local coordinates and where h denotes step size. Let x_k, $k = 1, \ldots, n-1$ be distinct points in $(0, h]$ and define partial extensions, Γ_k^{ext}, as $\Gamma_k^{\text{ext}} = \{(x, y(x)) : 0 \leq x \leq x_k\}$. The coefficients of the polynomial describing an extension are found by requiring that the mode II stress intensity factor is equal to zero for all partial extensions. Through numerical experiments, it was found that the most efficient choice if highly accurate results are desired is $n = 3$. If a crack grows from a pre-existing crack so that a kink develops, the leading term describing the crack shape close to the kink will, in a local coordinate system, be $x^{3/2}$. We therefore allow the crack extensions to contain such a term in addition to the monomial terms. The discontinuity in the crack growth direction at a kink, the kink angle, is determined by requiring that the mode II stress intensity factor should be equal to zero for an infinitesimal extension of the existing crack. To implement the scheme, accurate values of the stress intensity factors and T-stress are needed in each step of the simulation. These fracture parameters are computed using a previously developed integral equation of the second kind.

Key words: stress intensity factor; integral equation; crack growth; fast multipole method

1 Introduction

The present paper will study the problem of simulating quasi-static crack growth in two-dimensional linearly elastic specimens. One can envisage numerous practical situations where knowledge of the path a crack will follow under general loading is of interest. For example, properties of composite materials can be evaluated, and information can be obtained regarding the influence of different cracks on the life span of a certain specimen. The mathematical side of crack growth problems is very complex, as discussed in Friedman, Hu, and Velazquez [1]. We assume that the cracks we study grow quasi-statically, which means that dynamic effects can be neglected. We also assume that the cracks grow under mode I symmetry. Under these assumptions, a growing crack will follow a path such that the mode II stress intensity factor always is equal to zero. The problem of simulating a crack growing in such a way can be seen as a non-standard free boundary problem. Compared to typical free boundary problems studied in the literature [2], the problem under consideration here differs in at least two ways [1]. First, instead of having some condition on the entire free boundary, we only have a condition of vanishing mode II stress intensity factor at the crack tip. Second, once the

[1] This work was supported by the Swedish Research Council under contract 621-2004-3672 to Johan Helsing.

crack tip has passed through a point, the boundary at that point remains fixed. To the best of our knowledge, proving well-posedness of the problem at hand is an open problem.

Crack growth simulations in different settings have been conducted in a vast number of earlier papers. Examples are [3-21]. A majority of these schemes simulate the growing crack as a succession of straight pieces. The simulated crack will therefore contain kinks and the order of such a scheme cannot be higher than one. There exist relatively few papers that consider crack propagation that is not piecewise straight. Examples are given by [8, 9, 14, 19]. Studies of convergence of crack paths under mesh refinement are also scarce. Examples are given by [4, 11, 19]. In the present paper the goal is to construct a scheme that is of second order in the step size. That is, when the path taken by a quasi-statically growing crack in a certain setup is simulated, the error in the crack tip position at the end of the simulation is proportional to the square of the step size. Such a second order scheme is achieved using non-straight crack extensions together with a combination of different numerical and analytical methods.

The paper is organized as follows. Section 2 reviews different approaches used in quasi-static crack growth simulations. Section 3 discusses the new developments of the present paper. The numerical implementation of those developments is also mentioned briefly in Section 3. Section 4 contains the background of our numerical methods for the computation of stress intensity factors and T-stress. The key element is a boundary integral equation of the second kind, which has been studied in the earlier papers [22] and [23]. Finally, Section 5 contains several numerical experiments that verify the quality of our approach.

2 Review of previous work

In the present section we will discuss different approaches to the problem of simulating quasi-static crack growth. The first approaches that we mention are straightforward and comparatively easy to implement. These approaches, however, turn out to be suboptimal if accurate results are desired. The reason for mentioning them anyway is that they are the most commonly used methods in earlier papers. If one wants to obtain a highly reliable solution in a fast way, more involved approaches must be used. These are also discussed below.

The main interest in a majority of the papers where crack growth simulations are performed is usually not to construct efficient schemes for non-straight crack extensions. Instead, the focus is typically on the construction of algorithms for the computation of the stress field and fracture parameters rather than developing methods that specifically concern the problem of crack growth. The problem of simulating crack growth is only considered to be an application of the stress field algorithm. Many papers where finite element methods are used, focus on the construction of schemes that try to minimize the amount of remeshing.

2.1 Examples of explicit crack growth direction criteria

Assume that we have the situation depicted in Fig. 1 and that we want to determine the direction, θ, the crack would take initially if it starts growing in a quasi-static fashion from γ^{t}. The most commonly used crack growth direction criterion is presented in [24], where it is suggested that a crack will grow in a direction perpendicular to the maximum principal stress. This criterion for crack growth direction is usually called the *maximum circumferential stress criterion*, the *maximum hoop stress criterion* or the *maximum principal stress criterion*. From the expressions describing the stress field close to a crack tip, see for instance page 520 of [24], it follows that the direction with maximum circumferential stress is given by the solution to

$$K_{\mathrm{I}} \sin(\theta) + K_{\mathrm{II}}(3\cos(\theta) - 1) = 0, \tag{1}$$

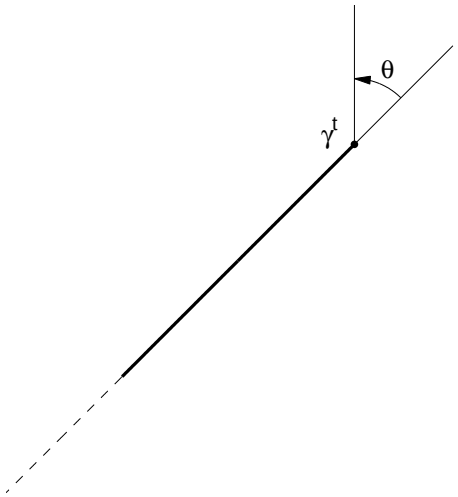

Figure 1: Part of an existing crack with tip at γ^t. The dashed line indicates that the existing crack continues in that direction.

where θ is defined in Fig. 1, and where K_{I} and K_{II} denote the mode I and mode II stress intensity factors for crack tip γ^t, respectively. Thus, to be able to apply this criterion, one has to compute the stress intensity factors. Two other well known crack growth direction criteria are given in [25] and [26]. The criterion in [25] is usually called the *minimum strain energy density criterion* and suggests that a crack will grow in a direction that minimizes the strain energy density factor. The criterion in [26] is usually called the *maximum energy release rate criterion* and suggests that a crack will grow in a direction which maximizes the energy release rate. This criterion leads to an identical crack growth direction as the maximum circumferential stress criterion [26]. In Reference [7] it is pointed out that one merit of using the maximum energy release rate criterion rather that the maximum circumferential stress criterion is that the latter criterion requires that the stress intensity factors can be computed accurately, while the former criterion can use information about the stress field further away from the crack tip. Knowledge of the stress intensity factors is not needed. Application of the maximum circumferential stress criterion is however more straightforward since one only has to solve Eq. (1) in order to get a growth direction, while the maximum energy release rate criterion is more computationally expensive [7]. According to some authors [5, 6], the minimum strain energy density criterion is less appropriate than the other two criteria. Examples of references where the maximum circumferential stress criterion is used are [3, 5, 11, 12, 13, 15, 16]. Examples of references where the minimum strain energy density and maximum energy release rate criteria are used are [4, 17] and [6, 7], respectively.

We will now mention a serious shortcoming of the maximum circumferential stress criterion, which is the most commonly used criterion in the literature. Since the other two criteria mentioned above are similar to this criterion, they exhibit similar shortcomings. In our opinion, the use of the maximum circumferential criterion for simulating crack growth is questionable in many situations since this criterion does not give the correct kink angle, see Section 8.6 of [27]. For a visualization of this problem see Fig. 2, where crack growth has been simulated using straight extensions in combination with the maximum circumferential stress criterion. That this criterion leads to an incorrect kink angle is a consequence of the fact that it only considers the situation before the crack actually grows. One could say that it is an explicit criterion rather than an implicit one. The kink angle for the first step using this criterion turns out to be approximately 37.92° for the situation shown in Fig. 2. From the figure one

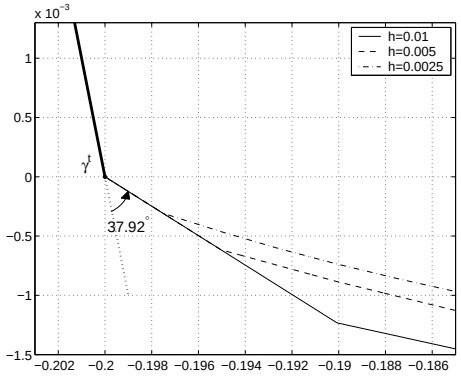

Figure 2: Example of a crack growth simulation using straight extensions in combination with the maximum circumferential stress criterion. The kink angle for the first step according to that criterion is approximately 37.92° in the present situation. The original crack is shown as a bold line. Details regarding the setup used in the figure are given in Section 5.1. The step size is denoted by h.

can clearly see that this angle is too small and as the step size, h, is decreased, the kink angle for the second step does not tend to zero.

2.2 An implicit crack growth direction criterion

A more appropriate approach than those presented in the previous section is to investigate the stress field when the crack has been allowed to grow an infinitesimal distance. One could say that this is an implicit approach. In order to proceed we need to introduce the principle of local symmetry [28] which assumes that the leading order of the expansion of the stress field around the tip of a quasi-statically growing crack is symmetric. This in turn has the consequence that

$$K_{\mathrm{II}} = 0. \tag{2}$$

In other words, the crack growth problem consists of constructing a growing crack that fulfills Eq. (2) as closely as possible. Denote an existing crack by $\Gamma_c^{(1)}$. We will use the notation K_{II} when we are referring to the mode II stress intensity factor of an existing crack. Below, we will frequently consider the situation when some extension is to be added to an existing crack. Before the crack is actually extended, an appropriate form of the extension must be found. Denote a possible extension by Γ_c^{pos}. By the notation k_{II} will be meant the mode II stress intensity factor for a possible extension, $\Gamma_c^{(1)} \cup \Gamma_c^{\mathrm{pos}}$. Once an appropriate extension has been found, the crack is extended. Denote the extended crack by $\Gamma_c^{(2)}$. If $\Gamma_c^{(2)}$ then is to be extended with yet another extension, the crack $\Gamma_c^{(2)}$ will now be seen as an existing crack, and so on. The condition of vanishing mode II stress intensity factor can be used as a crack growth direction criterion. To this end one has to determine the direction of crack growth that gives $k_{\mathrm{II}} = 0$ for an infinitesimal crack extension. One way to find that direction is by investigating an infinite crack with a finite kink, as depicted in Fig. 3. The problem consists of computing the stress intensity factors for the crack in Fig. 3 when known traction is applied at infinity and when the crack is traction free. One method that can be used to solve such a problem analytically is presented in [29] and [30]. The main components of the method described there are: The Mellin transform is applied to the equilibrium conditions, to Hooke's law, and to the boundary conditions. This will transform the problem into a factorization problem for matrices, the solution of which is given in [29]. Once the factorization problem

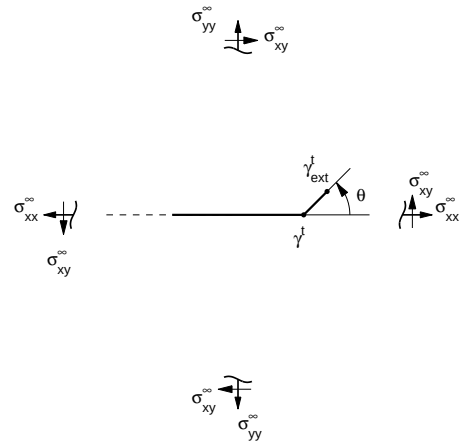

Figure 3: The setup studied in [30] to compute stress intensity factors at the tip of an infinitesimal kink. The dashed line indicates that the crack extends towards infinity in that direction. The length of the kink is unity.

has been solved, stress intensity factors at crack tip $\gamma^{\mathrm{t}}_{\mathrm{ext}}$, defined in Fig. 3, can be obtained directly from the Mellin transformed quantities, see Section 4.9 of [27]. Numerical results regarding the solution of the problem at hand can be found in [30], where the mode II stress intensity factor, k_{II}, for crack tip $\gamma^{\mathrm{t}}_{\mathrm{ext}}$, is given in the form

$$k_{\mathrm{II}}(\theta) = R_{21}(\theta)K_{\mathrm{I}} + R_{22}(\theta)K_{\mathrm{II}}, \tag{3}$$

where θ is as defined in Fig. 3, where K_{I} and K_{II} are stress intensity factors for the crack without the kink, and where $R_{21}(\theta)$ and $R_{22}(\theta)$ are functions that are computed numerically in [30]. Given K_{I} and K_{II}, Eq. (3) can now be used as a crack growth direction criterion by computing the angle θ that gives $k_{\mathrm{II}} = 0$. As an example, Eq. (3) gives a kink angle of approximately 39.57° for the situation in Fig. 2. This angle is the correct one to use. Numerical experiments show that, using this criterion and letting the step size tend to zero, the kink angle for the second step of the simulation also tends to zero. If instead the maximum circumferential stress criterion is used while letting the step size tend to zero, the kink angle for the second step tends to $39.57^\circ - 37.92^\circ = 1.65^\circ$.

Once the functions $R_{21}(\theta)$ and $R_{22}(\theta)$ have been computed, Eq.(3) can be used as a crack growth direction criteria for any cracked specimen. The functions $R_{21}(\theta)$ and $R_{22}(\theta)$ are universal in the sense that they do not depend on the setup under consideration.

2.3 The leading non-monomial term

Numerical crack growth simulations are typically performed in a stepwise manner, where an extension to the already existing crack is added in each step. When crack growth is simulated using straight extensions, the only parameter that has to be determined in each step is the current direction of crack growth. With such an approach, each extension can be described using a linear function. In the preceding section a method to determine the correct form of a first degree extension, using universal functions, was discussed. A natural question to ask is if similar universal functions can be found that describe asymptotically correct higher order terms of an extension. The answer to that question can be found in [1] and [31]. It turns out that universal functions that describe the leading non-linear term of an extension can be found for a crack that at onset of crack growth develops a kink, see page 466 of [31]. The setup in

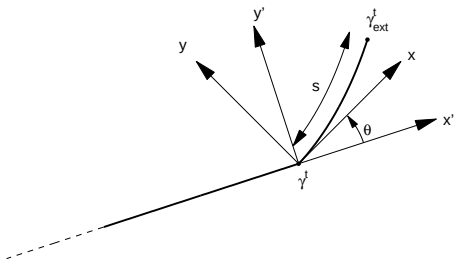

Figure 4: The non-straight extension discussed in [31]. The crack tip of the existing crack is denoted by γ^t, while the crack tip of the extension is denoted by γ^t_{ext}. By s is meant the arclength of the extension. The dashed line indicates that the existing crack continues in that direction.

Fig. 2 is an example of such a situation, where a kink will typically form at γ^t. As discussed in both [1] and [31], all other higher order terms of the crack shape depend on the setup under consideration and those terms cannot be described by a universal function. Assume that an existing crack is extended from crack tip γ^t in the fashion depicted in Fig. 4. As discussed in Appendix A of [32], it is natural and necessary to assume that the extension in a local coordinate system centered at γ^t and aligned with the crack growth direction given by Eq. (3), can be described by

$$y(x) = d_{3/2}x^{3/2} + d_2x^2 + O(x^{5/2}), \tag{4}$$

where $d_{3/2}, d_2 \in \mathbb{R}$. Similar crack extension shapes are discussed in [33] for a crack growing quasi-statically in mode III. In [31] and [32] it is also derived that the stress intensity factor k_{II} at crack tip γ^t_{ext}, for an extension of the type (4), can be expanded as

$$k_{\text{II}}(s) = c_0 + c_{1/2}s^{1/2} + c_1 s + O(s^{3/2}), \tag{5}$$

where $c_0, c_{1/2}, c_1 \in \mathbb{R}$, and where s is the arclength of the extension, see Fig. 4. The coefficient c_1 contains a non-universal term and will not be considered in what follows, while the other two coefficients in Eq. (5) are given by [31]

$$c_0 = F_{21}(\theta)K_{\text{I}} + F_{22}(\theta)K_{\text{II}}, \tag{6}$$

$$c_{1/2} = G_2(\theta)T + d_{3/2}\left(H_{21}(\theta)K_{\text{I}} + H_{22}(\theta)K_{\text{II}}\right), \tag{7}$$

where K_{I} and K_{II} are stress intensity factors for the existing crack and where T denotes T-stress for the existing crack. The functions $F_{21}(\theta)$, $F_{22}(\theta)$, $G_2(\theta)$, $H_{21}(\theta)$, and $H_{22}(\theta)$ are universal functions that can be computed numerically. Actually, the functions $F_{21}(\theta)$ and $F_{22}(\theta)$ are identical to the functions $R_{21}(\theta)$ and $R_{22}(\theta)$ of Eq. (3). The only thing that differs is the method used to derive them. This fact will be discussed further in Section 3. From condition (2) we know that $k_{\text{II}}(s)$ is equal to zero for the analytically correct crack extension. In other words, the coefficients appearing in the expansion of Eq. (5) are also equal to zero for the analytically correct extension. The condition $c_0 = 0$ is identical to the condition $k_{\text{II}}(\theta) = 0$ from Eq. (3) and can be used as a crack growth direction criterion. From the condition $c_{1/2} = 0$ one can in a similar manner obtain the asymptotically correct value of $d_{3/2}$ of Eq. (4). In Section 3 we will discuss the computation of the different functions appearing in Eqs. (6) and (7), and the use of them in our crack growth scheme.

2.4 Non-straight extensions in the literature

As mentioned in Section 1, there are comparatively few papers that consider the problem of simulating crack growth using extensions that are not straight. For instance, in [14] the crack growth direction for the first step is determined using the maximum circumferential stress criterion, while the direction for subsequent steps are determined using the assumption that $k_{\rm II}$ should be zero each time the crack has been extended. The crack extensions used in [14] consist of circular arcs. A similar approach is taken in [9]. In order to find an extension that gives a small value of $k_{\rm II}$, an iterative procedure is used [9, 14]. In Stone and Babuška [19], an approach that is similar to our scheme is taken. The crack extensions are assumed to have the form d_2x^2 in a local coordinate system at the crack tip, compare Fig. 4. To determine an appropriate value of the coefficient d_2, the secant method is used in order achieve a value of $k_{\rm II}$ at the crack tip $\gamma_{\rm ext}^{\rm t}$ that is as small as possible. The first step of the simulations in [19] is allowed to produce a kink, the angle of which is determined using the maximum circumferential stress criterion. Since $k_{\rm II}$ will be small for the first step, the kink angle is assumed to be zero for the subsequent steps. Interestingly, in [19] a potential modification of their scheme is discussed, where they point out the possibility of approximating crack extensions using polynomials with higher degree, n, than two. Denote an extension by $\Gamma^{\rm ext}$, where $\Gamma^{\rm exp} = \{(x, y(x)) : 0 \leq x \leq h\}$, where x and y are local coordinates as in Fig. 4 and where h denotes step size. Let x_k, $k = 1, \ldots, n-1$ be distinct points in $(0, h]$ and define the *partial extensions*, $\Gamma_k^{\rm ext}$, as $\Gamma_k^{\rm ext} = \{(x, y(x)) : 0 \leq x \leq x_k\}$. The coefficients of the polynomial describing an extension should be determined so that the value of $k_{\rm II}$ is small for all partial extensions. In [19] it is however claimed that such an approach, using extensions consisting of third degree polynomials and a certain step size, is similar to taking two steps of half the step size using polynomials of degree two. It is also claimed that using higher degree polynomials in x will not be competitive due to the increased computational cost of such an approach. Below, we will show that those claims are not necessarily true. Our numerical experiments indicate that using extensions which consist of polynomials of degree three in x is significantly more accurate than taking two steps using second degree polynomials. The overall computational cost of reaching a certain accuracy in the solution turns out to be lower using third degree polynomials instead of second degree polynomials.

Stone and Babuška [19] is one of a few papers in the literature that present numerical results showing the convergence of the simulated crack paths as the step size is decreased. Figure 18 in [19] shows the convergence of the crack path towards a reference crack, which was obtained using extrapolation. That figure indicates that the method used in [19] approximately is a first order method. That is, the distance from the crack tip of the simulated crack to the tip of the reference crack seems to decrease linearly with the step size. Below, we show that our algorithm, when using extensions in the form of second degree polynomials, seems to be of order 1.5 for at least one situation. One reason for the difference between the present results and those in [19] might be that the step size used in [19] is too large for the asymptotic order of the method to be seen.

3 The new developments

As mentioned in Sections 1 and 2, a common approach in the literature is to simulate quasi-static crack growth using straight extensions. Two obvious downsides with straight extensions are: First, kinks will be introduced along the propagating crack. Obtaining accurate results is typically more costly, from a computational point of view, when the crack contains kinks. Second, the order of such a method will surely never be higher than one. Here we aim at constructing a scheme that both makes the kink angles very small after each crack extension and has higher order that one. This section summarizes the main features of our scheme.

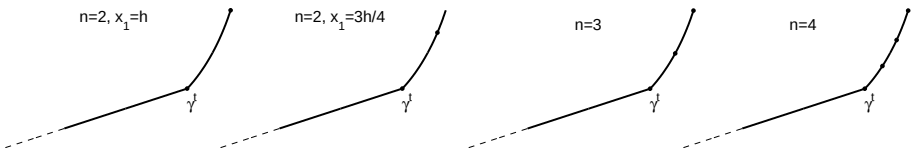

Figure 5: The points, x_k, which define the partial extensions, for different values of n. The crack tip of the existing crack is denoted by γ^t.

3.1 Finding appropriate extensions

For a crack that starts growing in a quasi-static fashion, a kink will typically appear, see Fig. 2. Note that the appearance of this kink is a consequence of the problem formulation rather than an effect of the algorithm used. The kink angle is determined from the criterion $c_0 = 0$, where c_0 is defined by Eq. (6). Furthermore, the dominant term of the crack shape close to a kink is given by $d_{3/2}x^{3/2}$, compare Eq. (4). The asymptotically correct value of the coefficient $d_{3/2}$ can be obtained from the condition $c_{1/2} = 0$, where $c_{1/2}$ is defined by Eq. (7). The two criteria $c_0 = 0$ and $c_{1/2} = 0$ are important for the first step of a crack growth simulation. For the subsequent steps, the mode II stress intensity factor will be non-zero but small after each step. This has the consequence that the kink angle, θ, and the coefficient $d_{3/2}$ also will be small for the subsequent steps. We compute and use values of θ and $d_{3/2}$ for all steps, even though other parameters will be the dominant ones for steps other than the first. Once the values of θ and $d_{3/2}$ have been determined for a certain step, we will assume that the extension, in the local coordinate system of Fig. 4, has the form

$$y(x) = d_{3/2}x^{3/2} + \sum_{i=2}^{n} d_i x^i, \quad x \in [0, h], \tag{8}$$

where h denotes the step size and where $n \geq 2$. Extensions of the type defined by Eq. (8) are used in all steps of a simulation. Note that even if a constant step size is used, the arclength of the extensions will vary slightly from step to step. The coefficients d_i, $i = 2, \ldots, n$ of Eq. (8) must be determined in order to get an appropriate form of the extension. According to the criterion (2) the coefficients should be such that the value of the mode II stress intensity factor is small for each partial extension. See Section 2 for a definition of the concept partial extension. In order to find suitable coefficients d_i for a certain extension we use Broyden's method, which is a modification of the secant method applicable to systems of equations. For one dimensional problems Broyden's method is identical to the secant method, which is the method used in Stone and Babuška [19] to compute d_2. Let $\mathbf{d}_0$ be a vector of dimension $n-1$ containing initial guesses for the $n-1$ unknown coefficients of Eq. (8). For simplicity, one can use the initial guess $d_i = 0$, for all i. Let $\mathbf{f}(\mathbf{d}_j)$ denote a vector containing values of the mode II stress intensity factor for all the $n-1$ partial extensions. For $n = 2$ we choose either $x_1 = h$ or $x_1 = 3h/4$. For $n > 2$ we choose the points x_k as $x_k = kh/(n-1)$, $k = 1, \ldots, n-1$, see Fig. 5. Pseudo-code for Broyden's method in this setting is

```
j=0
while norm(f(d_j))>tolerance
  Solve B_j*s_j=-f(d_j)
  d_jplus=d_j+s_j
  y_j=f(d_jplus)-f(d_j)
  B_j=B_j+scalprod(y_j-B_j*s_j,s_j)/scalprod(s_j,s_j)
  d_j=d_jplus
```

```
  j=j+1
end
```

where `scalprod` denotes a function that computes the scalar product and where `B_j` for $j = 0$ can be chosen as the $(n-1) \times (n-1)$ identity matrix. In each iteration k_{II} has to be computed for the $n-1$ partial extensions. In the numerical experiments below, the tolerance was typically set to 10^{-10}.

3.2 Computation of the universal functions

We will now discuss the computation of the functions appearing on the right-hand sides of Eqs. (6) and (7). As mentioned in Section 2.3, the functions $F_{21}(\theta)$ and $F_{22}(\theta)$ are identical to the functions $R_{21}(\theta)$ and $R_{22}(\theta)$ of Eq. (3). Accurate values of those functions can be found in both [30] and [31]. Since we desire even higher accuracy than found in these references we have to perform new computations of the function values of interest. In [30] a method based on [29], as described briefly in Section 2.2, was used. In [31] a completely different method was used. It deserves to be mentioned that for the computation of the functions $F_{21}(\theta)$ and $F_{22}(\theta)$ we implemented both methods. Below, we have chosen to use the method suggested in [31], despite being slower than the method of [30] with our implementation, since it can be used to compute also the functions appearing on the right hand side of Eq. (7). The absolute differences between the obtained function values, using the two methods, was found to be on the order of 10^{-15}. For example, both methods gave $F_{21}(\pi/12) = 0.12812831601512$ and $F_{22}(\pi/12) = 0.94722714515556$. When implementing the method of [30] we noticed some minor misprints in that reference. On the left hand side of Eq. (20) in [30] is says $\Lambda\_(-1/2)$, while it should say $\Lambda_-^{-1/2}(-1/2)$, compare Eq. (4.5) in [29]. The last term within square brackets on the right hand side of Eq. (22) in [30] should be squared, compare the line below Eq. (4.4) in [29].

The method used in [31], to obtain the functions $F_{21}(\theta)$, $F_{22}(\theta)$, and $G_2(\theta)$, is to map a kinked crack conformally onto the unit circle. The exterior of the crack is mapped onto the exterior of the unit disk. A boundary integral equation for the computation of the stress field around the crack is derived for the mapped problem. Two integral equations for the situation when the kink is infinitesimally short is obtained by expanding appearing quantities in powers of the length of the kink. One of the two integral equations concerns the computation of $F_{21}(\theta)$ and $F_{22}(\theta)$, while the other concerns the computation of $G_2(\theta)$. In a similar, but more complicated fashion, an integral equation for the computation of $H_{21}(\theta)$ and $H_{22}(\theta)$ of Eq. (7) is also derived. Solving these integral equations is straightforward, except for one circumstance regarding the computation of the functions $H_{21}(\theta)$ and $H_{22}(\theta)$. This is discussed on page 490 of [31] and concerns the numerical computation of integrals of the type

$$\int_{\Gamma^-} \frac{f(\tau)\,\mathrm{d}\tau}{(\tau - z)^m},$$

where m is equal to either 2 or 3, where Γ^- in [31] is defined as $\Gamma^- = \cos(t) + \mathrm{i}/2 \sin(t)$, $-\pi \leq t \leq 0$, and where z is some point on the unit circle. The construction of Γ^- in [31] is not optimal from a numerical point of view. If an adaptive approach is taken, where the mesh is refined for t close to $-\pi$ and 0, discretization points on Γ^- will end up very close to some points, z, of the unit circle. Further refinement of the mesh only makes the situation worse. This problem is fortunately easy to avoid by defining Γ^- as for instance $\Gamma^- = t + \mathrm{i}(-1/2 + 3/4t^2 - 1/4t^4)$, $-1 \leq t \leq 1$ instead. This is the construction used here when computing the functions $H_{21}(\theta)$ and $H_{22}(\theta)$.

The functions $F_{21}(\theta)$, $F_{22}(\theta)$, $G_2(\theta)$, $H_{21}(\theta)$, and $H_{22}(\theta)$ can be computed once and for all in a preprocessing step. To this end, the interval $[0, \pi/2]$ was subdivided into 100 equally long

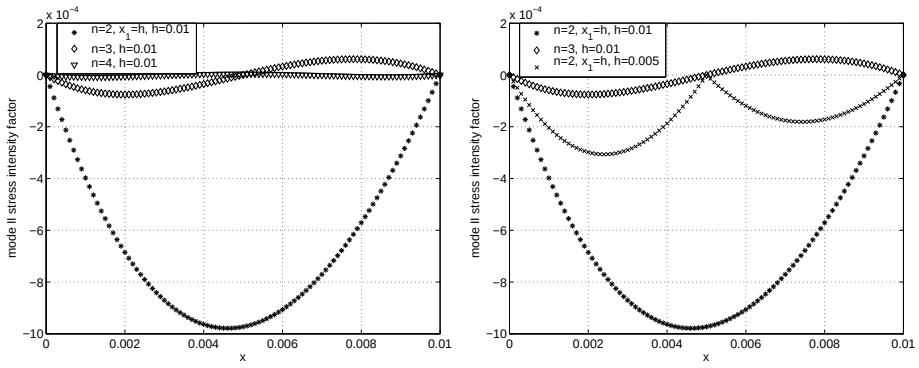

Figure 6: Investigation of $\overline{K}_{\mathrm{II}}$ using extensions of the type shown in Eq. (8). The quantity $\overline{K}_{\mathrm{II}}$ is a vector containing values of the mode II stress intensity factor for 100 partial extensions. Extensions with different values of n are compared. The step size is denoted by h.

subintervals. In each subinterval, the functions of interest were computed at the points corresponding to the nodes of 8-point Gauss-Legendre quadrature. In the numerical experiments below these computed values are interpolated in each subinterval in order to obtain the function values needed in the simulations. The functions $F_{22}(\theta)$ and $H_{21}(\theta)$ are even, while $F_{21}(\theta)$, $G_2(\theta)$, and $H_{22}(\theta)$ are odd. Furthermore, the largest possible kink angle is approximately $77°$, and it is therefore sufficient to compute the functions for $\theta \in [0, \pi/2]$.

3.3 Differences between the present scheme and Reference [19]

The differences between the present crack growth scheme and the one in Stone and Babuška [19] include:

- Our scheme uses higher order extensions than in [19], where only second degree polynomials are used.
- We use a more suiting crack growth direction criterion. In [19] the maximum circumferential stress criterion, Eq. (1), is used for the first step while we use $c_0 = 0$ for all steps, compare Eq. (6). See Fig. 2 for an example of the relevance of using an appropriate crack growth direction criterion.
- Here, the analysis from [31] has been used to obtain the asymptotically correct expression for the leading non-linear term of extensions adjacent to a kink. That is, the coefficient $d_{3/2}$, appearing in Eq. (8), is computed in each step by requiring that $c_{1/2} = 0$, compare Eq. (7). In [19] this term is omitted.
- In [19], partial extensions with $x_1 = h$ is used for $n = 2$. We prefer to use partial extensions with $x_1 = 3h/4$ for $n = 2$, see Fig. 5. This results in slightly more accurate results, as will be seen in Section 5.1.
- We use a boundary integral equation of the second kind, see Section 4, to compute parameters needed by the crack growth scheme. In [19] a finite element method is used for the same purpose.

3.4 Properties of different extensions

In order to investigate the behaviour of different types of extensions, a series of numerical experiments were performed. Briefly, the setup used here concerns the second step of the

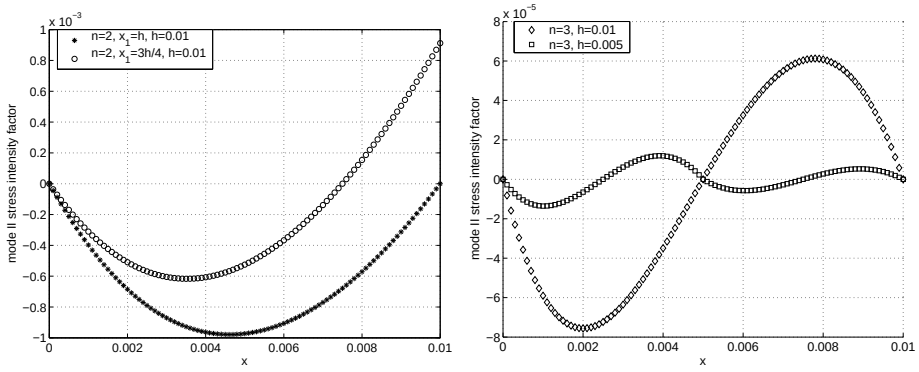

Figure 7: Left, investigation of the impact on $\overline{K}_{\mathrm{II}}$ of the choice of x_1 when $n = 2$. Right, the values of $\overline{K}_{\mathrm{II}}$ when $n = 3$, using different step sizes, h. The quantity $\overline{K}_{\mathrm{II}}$ is a vector containing values of the mode II stress intensity factor for 100 partial extensions.

crack growth simulation in Section 5.1. That is, one extension with step size $h = 0.01$ has already been added to the setup of Fig. 9. Extensions with different values of n were then added to that setup in accordance with the scheme described above. In doing so we either added one step with $h = 0.01$ or two steps with $h = 0.005$. As above, an extension is denoted by $\Gamma^{\mathrm{exp}} = \{(x, y(x)) : 0 \leq x \leq h\}$, where x and y are local coordinates as in Fig. 4. (note that for $h = 0.005$, an extension will consist of two steps in the present experiment). Then, values of the mode II stress intensity factor were computed for the partial extensions $\Gamma_k^{\mathrm{ext}} = \{(x, y(x)) : 0 \leq x \leq x_k\}$, where $x_k = kh/100$, $k = 1, \ldots, 100$. Denote a vector containing values of the mode II stress intensity factor for all partial extensions by $\overline{K}_{\mathrm{II}}$. Results from the different experiments can be seen in Figs. 6 and 7, and in Table 1. Note that the time and the number of iterations in the last two lines of Table 1 is the sum of the time and the number of iterations from two steps. We conjecture that the area defined by the different extensions in Figs. 6 and 7 is somehow connected with the quality of the extension. Some things should be noted from the table and the figures. First, the value of $\|\overline{K}_{\mathrm{II}}\|_\infty$ decreases quickly when the degree of the extensions is increased. For $n = 4$, the absolute value of the mode II stress intensity factor is less than 10^{-5} for all partial extensions. This means that we have found an extension that approximately fulfills the condition given by Eq. (2). That is, the mode II stress intensity factor is small for any partial extension, and not just for the partial extensions used by the crack growth scheme. From the right part of Fig. 6 it is also evident that taking one step using a third degree polynomial is better than taking two steps using second degree polynomials. Second, the value of $\|\overline{K}_{\mathrm{II}}\|_\infty$ decreases more for $n = 3$ than for $n = 2$, when the step size is decreased, compare right part of Fig. 6 and right part of Fig. 7. This indicates that the order of a scheme with $n = 3$ is higher than the order of a scheme with $n = 2$. In Section 5.1 we will apply the different possible extensions to the problem of simulating crack growth taking more steps than was done here. Such simulations will reveal that, with our implementation, extensions with $n = 3$ are preferable. Third, the area defined by the curve $\overline{K}_{\mathrm{II}}$ for $x_1 = 3h/4$ in the left part of Fig. 7 is smaller than the corresponding area for $x_1 = h$. This indicates that $x_1 = 3h/4$ might be preferable.

4 Equations and relations

Consider an isotropic linearly elastic specimen that occupies a bounded and simply-connected domain, D, in the plane, see Fig. 8. The problem under consideration here is the computation

Table 1: Results for different types of extensions and step sizes, h. The column denoted Iterations contains the number of iterations needed by Broyden's method to determine the coefficients appearing in the different extensions. The iterations where terminated when either $\|\mathbf{f}(\mathbf{d}_j)\|_2$ had reached 10^{-10}, or when the change in $\mathbf{f}(\mathbf{d}_j)$ between two consecutive iterations had stagnated. The final column shows the computational time (normalized with respect to the first line) needed to compute the coefficients of the different extensions. Note that for $h = 0.005$, two steps have been taken.

n	h	$\|\overline{K}_{\mathrm{II}}\|_\infty$	Iterations	Time
2	0.01	$9.8 \cdot 10^{-4}$	5	1.00
3	0.01	$7.6 \cdot 10^{-5}$	7	2.28
4	0.01	$8.6 \cdot 10^{-6}$	15	8.19
2	0.005	$3.1 \cdot 10^{-4}$	11	2.23
3	0.005	$1.4 \cdot 10^{-5}$	10	3.92

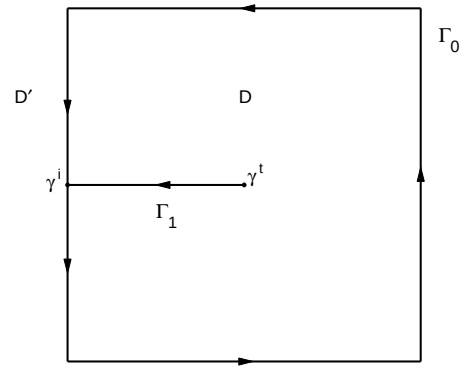

Figure 8: Example of a geometry with one edge crack. The figure shows the positive orientation of Γ and some notation. The crack tip is denoted by γ^{t} and the triple-junction by γ^{i}.

of the stress field in D when prescribed traction is applied to its oriented boundary, Γ. The exterior of D is denoted by D'. Furthermore, we assume that no body forces are present and that the applied traction is such that the specimen is in equilibrium. The specimens we will study contain a single traction free edge crack, Γ_1, and an outer boundary, Γ_0. That is, $\Gamma = \Gamma_0 \cup \Gamma_1$. The boundary will, in the present work, always contain four corners and a triple-junction, see Fig. 8. We have previously constructed integral equation methods for the numerical investigation of such setups, see [22] and [23]. Since the focus of attention in the present paper is on the modelling of quasi-static crack growth we will only briefly review some crucial material from [22] and [23].

The first step in the construction of an integral equation for the problem at hand is to use that Airy's stress function, $W(x, y)$, $(x, y) \in D \cup D'$, can be represented as

$$W(x, y) = \mathrm{Re}\,\{\bar{z}\varphi(z) + \chi(z)\}, \tag{9}$$

where $\varphi(z)$ and $\chi(z)$ are analytic functions of the complex variable $z = x + \mathrm{i}y$. As in [22] and [23], introduce $\Phi(z) = \varphi'(z)$, $\Psi(z) = \chi''(z)$, and the Cauchy potentials

$$\Phi(z) = \frac{1}{2\pi \mathrm{i}} \int_\Gamma \frac{\Omega(\tau)\,\mathrm{d}\tau}{\tau - z}, \quad z \in D \cup D', \tag{10}$$

$$\begin{aligned} \Psi(z) &= -\frac{1}{2\pi \mathrm{i}} \int_\Gamma \frac{\overline{\Omega(\tau)}\,\mathrm{d}\bar{\tau}}{\tau - z} - \frac{1}{2\pi \mathrm{i}} \int_\Gamma \frac{\bar{\tau}\Omega(\tau)\,\mathrm{d}\tau}{(\tau - z)^2} \\ &- \frac{1}{2\pi \mathrm{i}} \int_\Gamma \frac{\overline{n(\tau) t^{\mathrm{pr}}(\tau)}\,\mathrm{d}\tau}{\tau - z}, \quad z \in D \cup D', \end{aligned} \tag{11}$$

where $\Omega(z)$ is an unknown layer density on Γ, where $n = n(z)$ is the unit normal to Γ, and where $t^{\mathrm{pr}}(z)$ denotes prescribed traction. Once $\Phi(z)$ and $\Psi(z)$ have been determined, the stress state in $D \cup D'$ is known via the Kolosov formulae

$$\sigma_{xx} + \sigma_{yy} = 4\mathrm{Re}\,\{\Phi(z)\}, \quad z \in D \cup D', \tag{12}$$

$$\sigma_{yy} - \sigma_{xx} - 2\mathrm{i}\sigma_{xy} = 2(z\overline{\Phi'(z)} + \overline{\Psi(z)}), \quad z \in D \cup D'. \tag{13}$$

Using the potentials (10) and (11) it is possible to derive the following integral equation of the second kind for the problem at hand [22]

$$\left[I - \rho M_1 \rho^{-1} (M_3 + \chi_{\Gamma_0}(\mathrm{i}P_0 + \bar{z}Q))\right] \Omega(z) = \rho M_1 \rho^{-1} g(z), \quad z \in \Gamma. \tag{14}$$

The integral operators in Eq. (14) are defined by

$$M_1 f(z) = \frac{1}{\pi \mathrm{i}} \int_\Gamma \frac{f(\tau)\,\mathrm{d}\tau}{\tau - z}, \quad z \in \Gamma, \tag{15}$$

$$\begin{aligned} M_3 f(z) &= \frac{1}{2\pi \mathrm{i}} \int_\Gamma \frac{f(\tau)\,\mathrm{d}\tau}{\tau - z} + \frac{\bar{n}}{n} \frac{1}{2\pi \mathrm{i}} \int_\Gamma \frac{f(\tau)\,\mathrm{d}\tau}{\bar{\tau} - \bar{z}} \\ &+ \frac{1}{2\pi \mathrm{i}} \int_\Gamma \frac{\overline{f(\tau)}\,\mathrm{d}\bar{\tau}}{\bar{\tau} - \bar{z}} + \frac{\bar{n}}{n} \frac{1}{2\pi \mathrm{i}} \int_\Gamma \frac{(\tau - z)\overline{f(\tau)}\,\mathrm{d}\bar{\tau}}{(\bar{\tau} - \bar{z})^2}, \quad z \in \Gamma, \end{aligned} \tag{16}$$

$$Qf = \frac{1}{\pi \mathrm{i}} \int_\Gamma f(z)\,\mathrm{d}z, \tag{17}$$

and

$$P_0 f = -\frac{1}{2A} \mathrm{Re} \left\{ \int_{\Gamma_0} f(z) \bar{z}\,\mathrm{d}z \right\}, \tag{18}$$

where A denotes the area of D. By $\chi_{\Gamma_0}(z)$ is meant the characteristic function of Γ_0. Let γ^{t} denote the crack tip of Γ_1, and let γ^{i} denote the triple-junction, see Fig. 8. The function $\rho(z)$ appearing in Eq. (14) is defined by

$$\rho(z) = \begin{cases} -\rho_c(z), & z \in D \cup \Gamma_1, \\ \rho_c(z), & z \in D' \cup \Gamma_0, \end{cases} \tag{19}$$

where

$$\rho_c(z) = (z - \gamma^{\mathrm{i}})^{1/2} \cdot (z - \gamma^{\mathrm{t}})^{-1/2}. \tag{20}$$

The value of $\rho_c(z)$ for $z \in \Gamma$ is defined as the limit from the right relative to the orientation of Γ. Furthermore, we choose the branch given by a branch cut along Γ_1 and

$$\lim_{z\to\infty} \rho_c(z) = 1. \tag{21}$$

The right hand side of Eq. (14) is given by

$$g(z) = \frac{\bar{n}t^{\rm pr}(z)}{2} + \frac{\bar{n}}{n}\frac{1}{2\pi \mathrm{i}}\int_\Gamma \frac{n(\tau)t^{\rm pr}(\tau)\,\mathrm{d}\bar{\tau}}{\bar{\tau}-\bar{z}}, \quad z \in \Gamma. \tag{22}$$

Equation (14) was studied in [22]. In [23] a simple preconditioner, which we now will review, was derived for Eq. (14). Below, we use a Nyström scheme based on composite quadrature to discretize our integral equations. Assume that Γ has been partitioned into a number of quadrature panels in such a way that no panel contains either a corner or a triple-junction in its interior. Number the corners of Γ_0 from 1 to 4 and let the triple-junction have number 5. Let Γ_j^p be the union of the two (or three) quadrature panels closest to corner (or triple-junction) j. Define the operator

$$M_1^p f(z) = \begin{cases} \frac{1}{\pi \mathrm{i}}\int_{\Gamma_j^p} \frac{f(\tau)\,\mathrm{d}\tau}{\tau - z}, & z \in \Gamma_j^p, \quad j = 1,\ldots,5, \\ 0, & z \in \Gamma \setminus \bigcup_{j=1}^5 \Gamma_j^p. \end{cases} \tag{23}$$

The operator M_3^p is defined analogously. In [23] a preconditioned version of Eq. (14) was constructed as

$$\left[I - (I-P)^{-1}(\rho M_1 \rho^{-1}(M_3 + \chi_{\Gamma_0}(\mathrm{i}P_0 + \bar{z}Q)) - P)\right]\Omega(z) = (I-P)^{-1}\rho M_1 \rho^{-1} g(z), \quad z \in \Gamma, \tag{24}$$

where $P = \rho M_1^p \rho^{-1} M_3^p$. In the numerical examples below we solve Eq. (24). Introduce the complex valued stress intensity factor $K(\gamma^{\rm t})$ defined by $K(\gamma^{\rm t}) = K_{\rm I} + \mathrm{i}K_{\rm II}$, where $K_{\rm I}$ and $K_{\rm II}$ are the usual mode I and II stress intensity factors for the crack tip $\gamma^{\rm t}$. Using the solution $\Omega(z)$ of (24) the stress intensity factors can be computed as [34]

$$K(\gamma^{\rm t}) = \mathrm{i}\sqrt{2\pi}\,\overline{\lim_{z\to\gamma^{\rm t}}\left\{\frac{\Omega(z)}{\rho(z)}\right\}}\lim_{z\to\gamma^{\rm t}}\left\{\overline{\rho(z)}\sqrt{\delta s(z)}\right\}, \quad z \in \Gamma, \tag{25}$$

where $\delta s(z)$ is arclength measured from $\gamma^{\rm t}$. In Eq. (25) we have assumed that the orientation of the crack is away from $\gamma^{\rm t}$, as shown in Fig. 8. The T-stress, $T(\gamma^{\rm t})$, at a crack tip $\gamma^{\rm t}$ can be computed using [34]

$$T(\gamma^{\rm t}) = 2\mathrm{Re}\left\{\frac{\overline{n(\gamma^{\rm t})}}{n(\gamma^{\rm t})}\left(\gamma^{\rm t}\overline{\Phi'(\gamma^{\rm t})} + \overline{\Psi(\gamma^{\rm t})}\right)\right\}. \tag{26}$$

Accurate values of the stress intensity factors and the T-stress are needed in our crack growth scheme.

5 Numerical experiments

The numerical implementation for the computation of the stress field used here is very similar to the ones used in [22] and [23]. We therefore refer to those two papers for more details. In the present section we will solve the integral equation (24) using a Nyström scheme were the integrals are discretized using composite quadrature. The code was written in Fortran 77 and compiled using the Sun Fortran 77 compiler. All experiments were performed on a SunBlade 100 workstation.

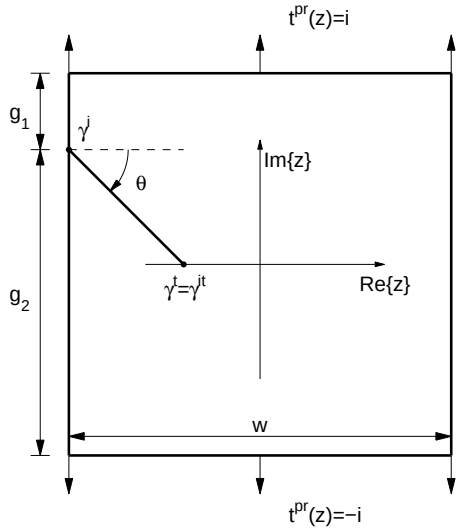

Figure 9: The initial configuration of the specimens studied in Sections 5.1 and 5.2. In all setups, $w = 1$ and $g_1 + g_2 = 1$. The values of the other quantities in the figure are defined in the text. Note that all specimens are centered at the origin of the complex plane.

The linear system of equations was solved using the GMRES iterative solver. A non-adaptive version of the fast multipole method was used to perform matrix-vector multiplications.

Around corners, at the triple-junction, γ^{i}, and around the kink that appears when the crack starts growing, an *a priori* adaptive approach was used when computing the stress field. Special quadrature as described in [23] was used around the corners and at the triple-junction, and therefore only a few levels of refinement are needed. At the kink more levels of refinement are needed, if one is aiming at obtaining highly accurate results, since the leading term of the solution, $\Omega(z)$, of Eq. (24) will be singular there [23].

The simulations below all concern setups similar to the one shown in Fig. 9. The upper and lower edges of the specimens are loaded with traction of unit magnitude, while the other edges are traction free. All specimens are assumed to be centered at the origin of the complex plane, and they all have width and height equal to one. That is, $w = 1$ and $g_1 + g_2 = 1$. The crack tip of the growing crack is denoted by γ^{t}. The crack tip of the initial configuration is denoted by γ^{it}. In order to assess the accuracy of different simulations we will use the computed intersection of the crack path and the imaginary axis, y_0, as a benchmark parameter, see Fig. 10. The simulations are discontinued once the growing crack has crossed the imaginary axis.

In all simulations we have used a constant step size, h.

5.1 A benchmark example

In this section we will study the path taken by the crack shown in Fig. 9 when it grows quasi-statically. The quantities in Fig. 9 are chosen as $g_1 = 0.2$, $g_2 = 0.8$, $\theta = \pi/4$, and $\gamma^{\mathrm{it}} = -0.2$. This setup was simulated using different polynomial degrees of the extensions and using different step sizes, see Fig. 11. Since the change in y_0 when decreasing the step size, for $n = 3$, turned out to decrease approximately in a quadratic fashion, we thought that it is reasonable to extrapolate the results for $n = 3$ in order to obtain an estimated reference value. Assuming that the error decreases quadratically when the step size is decreased, a

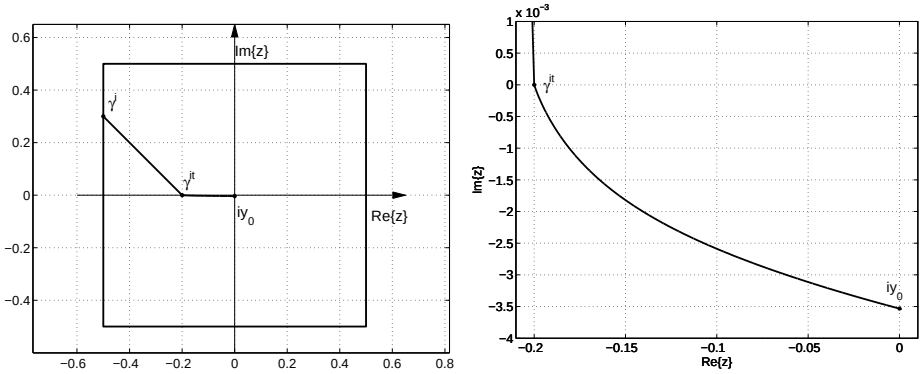

Figure 10: Left, the crack of the specimen discussed in Section 5.1 has been allowed to grow from the initial configuration until the crack tip has reached the imaginary axis. The intersection of the crack path and the imaginary axis is denoted by y_0. Right, a close-up of the crack path between the initial crack tip and the imaginary axis.

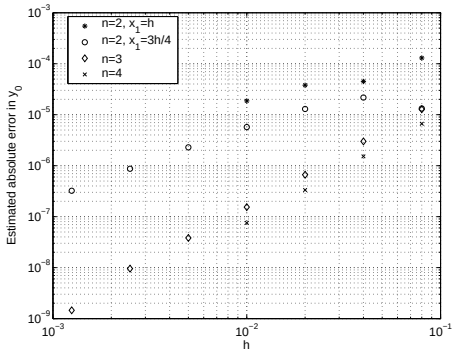

Figure 11: A convergence test where the crack defined in Section 5.1 has been allowed to grow until reaching the imaginary axis, compare Fig. 10. Different step sizes, h, and different degrees of the extensions, n, are compared.

simple Richardson extrapolation based on the values of y_0 for $h = 1 \cdot 10^{-2}$, $h = 5 \cdot 10^{-3}$, and $h = 2.5 \cdot 10^{-3}$ with $n = 3$ resulted in $y_0^{\text{ref}} = -0.0035325215$. This is the value used as reference in Fig. 11. Figure 11 has several interesting features. For instance, one can clearly see that extensions with third degree polynomials, $n = 3$, give significantly more accurate results than extensions with second degree polynomials, $n = 2$, for a given step size. The order of a scheme with $n = 3$ also seems to be higher than the order of a scheme with $n = 2$. According to Fig. 11, the order when using $n = 3$ seems to be approximately 2, while the order when using $n = 2$ seems to be approximately 1.5. In the figure one can also see that the use of $x_1 = 3h/4$ when $n = 2$, rather than $x_1 = h$, leads to slightly more accurate results. A final thing to note in Fig. 11 is that using fourth degree extensions, $n = 4$, does not give the significant improvement that Fig. 6, left part, hints at. One possible explanation for this behaviour might be that a term of the type $x^{5/2}$ needs to be included in Eq. (8) in order to obtain a method of higher order than 2.

The most accurate result obtained for the benchmark parameter was $y_0 = -0.0035325$, which we believe is correct in all the presented digits. This value corresponds to the diamond symbol in the lower left corner of Fig. 11. Regarding execution times for different choices of n one can say the following: In order to achieve an absolute error of about 10^{-6} in y_0, the

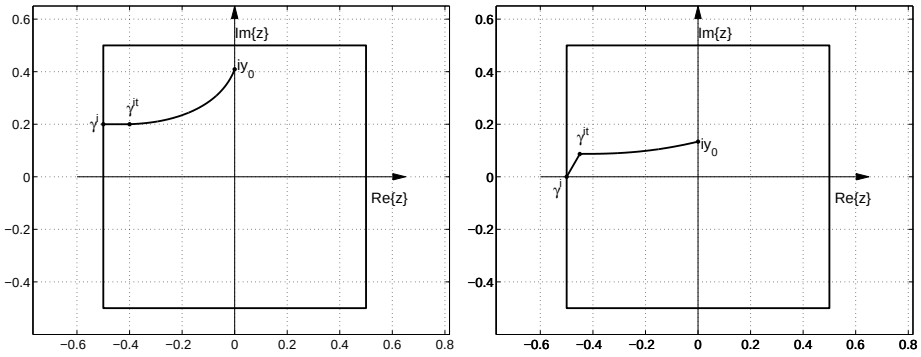

Figure 12: Examples of obtained crack paths for two of the specimens considered in Section 5.2. Left, the obtained crack path when the quantities in Fig. 9 were chosen as $g_1 = 0.3$, $g_2 = 0.7$, $\theta = 0$, and $\gamma^{\mathrm{it}} = -0.4 + 0.2\mathrm{i}$. Right, the obtained crack path when the quantities in Fig. 9 were chosen as $g_1 = 0.5$, $g_2 = 0.5$, $\theta = \pi/3$, and $\gamma^{\mathrm{it}} = -0.5 + 0.1\exp(\mathrm{i}\pi/3)$.

execution time needed if extensions with $n = 2$ are used is about 5 to 10 times longer than if extensions with $n = 3$ are used.

5.2 Further numerical examples

In addition to the benchmark example of the previous section, two simple parametric studies were performed. The first of these studies concerns the dependence of the crack path on the position of the edge crack. In this study the quantities in Fig. 9 are chosen as $g_1 = 0.5 - k \cdot 10^{-2}$, $\theta = 0$, and $\gamma^{\mathrm{it}} = -0.4 + \mathrm{i}k \cdot 10^{-2}$, where $k = 0, \ldots, 20$. The second study investigates the dependence of the crack path on the angle of a slanted edge crack. In this study the quantities in Fig. 9 are chosen as $g_1 = 0.5$, $\theta = k\pi/36$, and $\gamma^{\mathrm{it}} = -0.5 + 0.1e^{\mathrm{i}\theta}$, where $k = 0, \ldots, 12$. Examples of obtained crack paths are shown in Fig. 12. The results from the two parametric studies are shown in Fig. 13, where y_0 is defined as above. From the left part of Fig. 13 one can see that as soon as the initial crack is moved from the midpoint of the plate, its extended path tends to approach the closest horizontal plate edge. When the initial crack has been moved a distance of 0.2, the extended path will almost reach the horizontal boundary, before it reaches the imaginary axis. The behaviour shown in the right part of Fig. 13 is similar to the left part when it comes to the behaviour of y_0 as a function of $\mathrm{Im}\{\gamma^{\mathrm{it}}\}$. Consider the value of y_0 for $|g_1 - 0.5| = 0.05$ in the left part of Fig. 13, and the value of y_0 for $\theta = \pi/6$ in the right part of Fig. 13. In both these setups, $\mathrm{Im}\{\gamma^{\mathrm{it}}\} = 0.05$. The difference in y_0 between these two setups turned out to be approximately $8 \cdot 10^{-4}$. That is, the crack tip of the initial configuration has a stronger influence on the value of y_0 than the other characteristics of the crack. For instance, the distance between the triple-junctions of the two setups just mentioned is $5 \cdot 10^{-2}$.

6 Discussion

A scheme for efficient and accurate numerical simulation of quasi-static crack growth in two-dimensional elastic specimens has been presented. The scheme models the growing crack as a sequence of polynomial extensions. The shapes of the extensions are determined using the criterion that the mode II stress intensity factor vanishes when a crack grows quasi-statically under mode I symmetry. For situations when the crack develops a kink, the direction of crack growth, and the leading term of the crack shape were determined using analytical methods. In order to be able to use the scheme in a satisfactory manner, stress intensity factors and

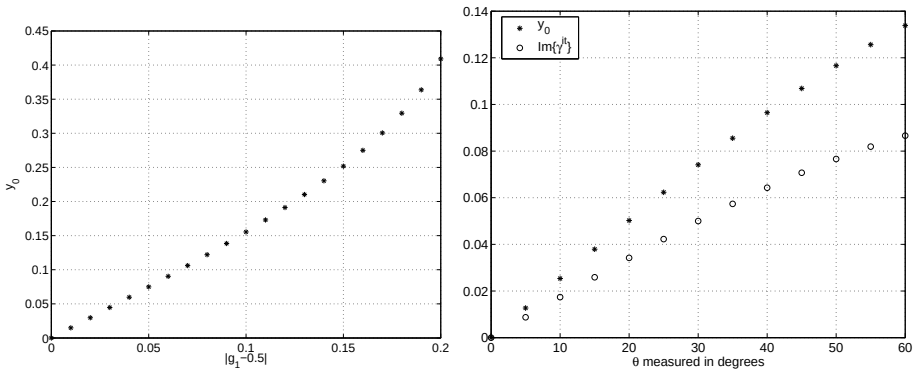

Figure 13: Results of the parametric studies of Section 5.2. Left, the intersection between the crack and the left edge of the plate was varied, while θ was held fixed at $\theta = 0$. Right, the intersection between the crack and the left edge of the plate was held fixed at $\gamma^{\mathrm{i}} = -0.5$, while θ was varied. The value of y_0 is compared to $\mathrm{Im}\{\gamma^{\mathrm{it}}\}$.

T-stress must be computed accurately. This was achieved using a previously developed second kind integral equation.

It is unlikely that one can obtain crack paths with higher accuracy than the accuracy of the stress intensity factors that are computed in each step of the simulation. The algorithm used to compute stress intensity factors in the present paper can typically compute these fracture parameters with relative errors of less than 10^{-10} for setups similar to the ones studied here. Therefore, it is probably the crack growth scheme, and not the stress intensity factor computations, that is the limiting factor when it comes to the accuracy of the obtained crack paths, for the step sizes used above.

With the present implementation, crack extensions in the form of third degree polynomials, defined in a local coordinate system, turned out to be the best choice. The order of a scheme with such extensions appears to be higher than one. It should be mentioned that to the best of our knowledge, proving convergence of schemes such as ours, is an open problem. To this end, questions that need to be answered are for instance: How does the accuracy in the stress intensity factors influence the crack path? What is the relation between the size of the mode II stress intensity factor for different partial extensions and the accuracy in the crack path? See Figs. 6, 7, and 11. Is it possible to modify the type of extensions used here, Eq. (8), in order to obtain a scheme with higher order than 2?

References

[1] Friedman A, Hu B, Velazquez JJL. The evolution of stress intensity factors in the propagation of two dimensional cracks. *European Journal of Applied Mathematics* 2000; **11**(5):453–471.

[2] Howison SD, Morgan JD, Ockendon JR. A class of codimension-two free boundary problems. *SIAM Review* 1997; **39**(2):221–253.

[3] Belytschko T, Black T. Elastic crack growth in finite elements with minimal remeshing. *International Journal for Numerical Methods in Engineering* 1999; **45**(5):601–620.

[4] Bittencourt TN, Wawrzynek PA, Ingraffea AR, Sousa JL. Quasi-automatic simulation of crack propagation for 2D LEFM problems. *Engineering Fracture Mechanics* 1996; **55**(2):321–334.

[5] Boselli J, Pitcher PD, Gregson PJ, Sinclair I. Numerical modelling of particle distribution effects on fatigue in $\mathrm{Al}-\mathrm{SiC_p}$ composites. *Materials Science and Engineering A* 2001; **300**(1-2):113–124.

[6] Bouchard PO, Bay F, Chastel Y. Numerical modelling of crack propagation: automatic remeshing and comparison of different criteria. *Computer Methods in Applied Mechanics and Engineering* 2003; **192**(35-36):3887–3908.

[7] Bush MB. The interaction between a crack and a particle cluster. *International Journal of Fracture* 1997; **88**(3):215–232.

[8] Datsishin OP, Marchenko GP. Quasistatic edge crack growth with non-self-balancing stresses at the edges. *Soviet Materials Science* 1991; **27**(4):379–385.

[9] Dobroskok A. On a new method for iterative calculation of crack trajectory. *International Journal of Fracture* 2001; **111**(3):L41–L46.

[10] Heintz P. On the numerical modelling of quasi-static crack growth in linear elastic fracture mechanics. *International Journal for Numerical Methods in Engineering* 2006; **65**(2):174–189.

[11] Huang R, Sukumar N, Prévost JH. Modeling quasi-static crack growth with the extended finite element method Part II: Numerical applications. *International Journal of Solids and Structures* 2003; **40**(26):7539–7552.

[12] Knight MG, Wrobel LC, Henshall JL, de Lacerda LA. A study of the interaction between a propagating crack and an uncoated/coated elastic inclusion using the BE technique. *International Journal of Fracture* 2002; **114**(1):47–61.

[13] Lee SH, Yoon YC. Numerical prediction of crack propagation by an enhanced element-free Galerkin method. *Nuclear Engineering and Design* 2004; **227**(3):257–271.

[14] Mogilevskaya SG. Numerical modeling of 2-D smooth crack growth. *International Journal of Fracture* 1997; **87**(4):389–405.

[15] Phongthanapanich S, Dechaumphai P. Adaptive Delaunay triangulation with object-oriented programming for crack propagation analysis. *Finite Elements in Analysis and Design* 2004; **40**(13-14):1753–1771.

[16] Rashid MM. The arbitrary local mesh replacement method: An alternative to remeshing for crack propagation analysis. *Computer Methods in Applied Mechanics and Engineering* 1998; **154**(1-2):133–150.

[17] Silveira NPP, Guimarães S, Telles JCF. A numerical Green's function BEM formulation for crack growth simulation. *Engineering Analysis with Boundary Elements* 2005; **29**(11):978–985.

[18] Stolarska M, Chopp DL, Moës N, Belytschko T. Modelling crack growth by level sets in the extended finite element method. *International Journal for Numerical Methods in Engineering* 2001; **51**(8):943–960.

[19] Stone TJ, Babuška I. A numerical method with a posteriori error estimation for determining the path taken by a propagating crack. *Computer Methods in Applied Mechanics and Engineering* 1998; **160**(3-4):245–271.

[20] Tabbara MR, Stone CM. A computational method for quasi-static fracture. *Computational Mechanics* 1998; **22**(2):203–210.

[21] Yan X. Multiple crack fatigue growth modeling by displacement discontinuity method with crack-tip elements. *Applied Mathematical Modelling* 2006; **30**(6):489–508.

[22] Englund J. Efficient algorithm for edge cracked geometries. *International Journal for Numerical Methods in Engineering*, available online 12 December 2005.

[23] Englund J. A Nyström scheme with rational quadrature applied to edge crack problems. *Submitted to Communications in Numerical Methods in Engineering.*

[24] Erdogan F, Sih GC. On the crack extension in plates under plane loading and transverse shear. *Journal of Basic Engineering* 1963; **85**:519–527.

[25] Sih GC. Strain-energy-density factor applied to mixed mode crack problems. *International Journal of Fracture* 1974; **10**(3):305–321.

[26] Nuismer RJ. An energy release rate criterion for mixed mode fracture. *International Journal of Fracture* 1975; **11**(2):245–250.

[27] Broberg KB. *Cracks and Fracture*. Academic Press: San Diego, 1999.

[28] Gol'dstein RV, Salganik RL. Brittle fracture of solids with arbitrary cracks. *International Journal of Fracture* 1974; **10**(4):507–523.

[29] Khrapkov AA. The first basic problem for a notch at the apex of an infinite wedge. *International Journal of Fracture* 1971; **7**(4):373–382.

[30] Melin S. Accurate data for stress intensity factors at infinitesimal kinks. *Journal of Applied Mechanics* 1994; **61**(2):467–470.

[31] Amestoy M, Leblond JB. Crack paths in plane situations-II. Detailed form of the expansion of the stress intensity factors. *International Journal of Solids and Structures* 1992; **29**(4):465–501.

[32] Leblond JB. Crack paths in plane situations-I. General form of the expansion of the stress intensity factors. *International Journal of Solids and Structures* 1989; **25**(11):1311–1325.

[33] Oleaga GE. On the path of a quasi-static crack in mode III. *Journal of Elasticity* 2004; **76**(2):163–189.

[34] Helsing J, Jonsson A. A seventh order accurate and stable algorithm for the computation of stress inside cracked rectangular domains. *International Journal for Multiscale Computational Engineering* 2004; **2**(1):47–68.